Geologia Croatica	63/1	75–91	11 Figs.	3 Tabs.		Zagreb 2010

Near vein metasomatism along propylitic veins in the Baksa Gneiss Complex, Pannonian Basin, Hungary

Krisztián Fintor[1], Tivadar M. Tóth[1] and Félix Schubert[1]

[1]Department of Mineralogy, Geochemistry and Petrology, University of Szeged, H-6701, Szeged, P.O. Box 651, Hungary;
(efkrisz@gmail.com; mtoth@geo.u-szeged.hu; schubert@geo.u-szeged.hu)

doi: 104154/gc.2010.05

Geologia Croatica

ABSTRACT

In many parts of the metapelitic (gneiss, mica schist) rock section of the Baksa Complex, significant wall-rock alteration is observable along the Ca-Al silicate veins, which show a *di* → *ep* ± *czo* →*sp* → *ab* ± *kfs* → *chl* → *adu* → *prh* → *py* → *cal* mineral sequence (FINTOR et al., 2009). These alterations appear as narrow (few cm thick) bleached margins beside thin veins, and broad alteration bands along thick veins where detailed epidotization and chloritization of the adjacent rock are recognizable. Based on petrographic and mineralogical examination of the altered wall-rocks, metasomatic zones with characteristic mineral paragenesis can be distinguished: Zone 1 (*ab* + *ttn* ± *ep*), Zone 2 (*ep* + *chl*+ *ttn* + *ab* ± *ser*), Zone 3 (*chl* + *ep* + *ser* + *rt* ± *ttn*), Zone 4 (*ser* ± *chl*). Bulk rock chemical analyses were made from the different metasomatic zones. The results show that fluid circulated in the propylitic veins caused metasomatic alteration of the wall-rock, with transport of considerable amount of Ca^{2+} toward the adjacent rocks. The hydrothermal leaching almost totally removed the K, Fe, Mg, and Mn ions from the wall rock. The main alteration processes are the epidotization and chloritization of biotite, and albitization of micas (muscovite + biotite) content of metapelites. Based on mobilization of different cations alteration was due to a near neutral fluid (~*pH* 5–7). The pervasive hydrothermal leaching caused significant secondary porosity (cavities) in the altered domains, which were partially filled by epidote. Fluid inclusions of cavity filling epidote indicate a similar character (T_h: 180–360 °C; Salinity: 0.2–1.6 mass% eq. NaCl) to that can be found in Ca-Al silicate veins. The alteration most probably occurred in the 360–480 °C temperature range as products of 'near vein metasomatism' and the altered rock can be related to the propylite metasomatic family.

Keywords: Baksa Complex, metasomatic zones, epidotization, chloritization, element mobilization, hydrothermal leaching, propylitization

1. INTRODUCTION

The wall rock alteration activity of hydrothermal fluids that circulate in fractures of crystalline rock bodies of the continental crust, has a significant role in different geological processes. Considerable secondary porosity may develop if metasomatic alteration is associated with leaching, and the locally increased porosity can play a pivotal role in the hydrological behaviour of otherwise low permeability crystalline rocks (MAZUREK et al., 2003; JAKOB et al., 2003). Another important aspect is that hydrothermal metasomatism can be frequently associated with formation of mineral deposits. Ore mineral deposition sometimes containing sulphide minerals (pyrite, chalcopyrite, pyrrhotite, and sphalerite) iron oxides (hematite, magnetite), or in other cases

precious metal minerals, can occur during hydrothermal metasomatism that mainly relates to magmatic intrusions (ZHARIKOV et al., 2007; SCHERBAN, 1996; GRYAZNOV, 1992; RUSINOV, 1989). Study of wall rocks where alteration is caused by hydrothermal fluid/rock interaction, may provide important information about the thermodynamic parameters (e. g.: *pH*, *Eh*, *T*, *P*, *X*) of fluids circulated in the rock body (PARSONS & LEE, 2000; KULLERUD, 2000; GRESENS, 1967; MEYER & HEMLEY, 1967).

The study area is the Baksa Complex which represents part of the metamorphic crystalline basement of the southwestern area of the Pannonian Basin. The Baksa-2 exploratory drillhole penetrated deeply into the Baksa Complex. With almost 100% core recovery, this exposed almost 1200 m of crystalline rocks of the basement. It is the most complete drillcore available from the crystalline basement of the Pannonian Basin.

A lot of evidence for postmetamorphic hydrothermal fluid migration and alteration can be observed in the drillcores of the Baksa-2 well. This alteration can be grouped into two main hydrothermal mineral parageneses. TARNAI (1997; 1998) provided detailed studies of a thick (6–7 cm) sulphide ore vein, cross cutting the metamorphic block. Ore paragenesis (*pyr+po+sp+hem+ccp+gn+pn*) and fluid inclusion studies of the vein filling minerals indicate a postmagmatic hydrothermal origin (TARNAI, 1998). The other assemblage suggests that the hydrothermal effect is the occurrence of Ca-Al silicate dominant fracture filling in several Baksa gneiss samples (SZEDERKÉNYI, 1979). Comprehensive examination of the latter vein-filling process was made by FINTOR et al. (2009) and they report the presence of sporadic pyrite crystals among the Ca-Al silicate minerals. Detailed mineral chemical analyses of pyrite crystals from both the Ca-Al silicate and the thick sulphide veins (FINTOR et al., 2009) exhibit similar Co/Ni ratios (1–5), which is in the range of pyrites formed in postmagmatic hydrothermal systems (PRICE, 1972).

In this study, detailed petrographic, bulk rock chemical, and fluid inclusion analysis of the altered wall rocks along the Ca-Al-silicate veins was undertaken. The aims are to detect the type and physicochemical conditions of metasomatism and element mobilization that occurred along the veins, and to determine the hydrological relationship between the alteration halos and the veins.

2. GEOLOGICAL SETTING

The Baksa Complex (BC) is located in the SW part of the Tisza Mega unit (Fig. 1), a microplate that forms the basement of South Hungary. The Tisza Mega unit was originally part of the European margin of Neo-Tethys and was separated from the European plate by opening of the Penninic Ocean (Alpine Tethys) (GÉCZY, 1973; HAAS & PÉRÓ, 2004). SZEDERKÉNYI (1996) divided the pre-Alpine basement complexes of the Tisza Mega unit into three major parts: the Paraautochton, Békés-Codru (BC) and Drava terrains, and related the BC to the Drava Terrain. The metamorphic formations of the complex do not outcrop. They are instead covered by thin (50–100 m) Tertiary and Quaternary sediments in the area of the Görcsöny Ridge. The crystalline schists of the Babócsa Complex border the BC to the west (Fig. 1). The Villány deep fracture zone (KASSAI, 1972), which has a NW–SE strike, separates the Baksa metamorphic block from the Mórágy Granite Complex, and Permo-Triassic sediments to the east. The Mecsekalja Tectonic Zone borders the complex in the north. It separates metamorphic rocks from non-metamorphic Mesozoic sediments of the Mecsek Mountains (Fig. 1). Further to the south, formations of the complex can be traced over the Slavonian regions, in the Papuk and Krndija Mountains.

Petrology and metamorphic evolution of the BC has been investigated by many researchers (RAVASZ-BARANYAI, 1969; SZEDERKÉNYI, 1976, 1983; ÁRKAI, 1985; ÁRKAI et al., 1999; KIRÁLY, 1996; HORVÁTH et al., 2003). The complex consists of polymetamorphic rocks, mainly gneiss, marble bearing mica-schist, dolomite, marble, and amphibolite. Five metamorphic events can be detected in the rocks of the BC. RAVASZ-BARANYAI (1969) detected a high pressure phase that was followed by a significant decompression. The peak conditions of this *P–T* path were around 1300–1500 MPa and 600–650 °C down to approximately 800 MPa and 500 °C (HORVÁTH et al., 2003). Peak conditions of the Barrowian event (SZEDERKÉNYI, 1976) occurring after the previous high pressure phase, were around 750±50 MPa, and 660±20 °C according to ÁRKAI et al. (1999), but KIRÁLY (1996) suggests conditions of 500–700 MPa and 540–650 °C. After the Barrowian event, the area underwent secondary albitization and isothermal decompression down to 440±20 MPa and 650±40 °C according to ÁRKAI et al. (1999) or < 200 MPa, 400–560 °C according to KIRÁLY (1996).

The isothermal decompression was followed by contact metasomatism related to aplite intrusions. These aplite dykes with unknown origin, caused considerable alteration but only in the carbonate rocks of the complex. Significant alteration products include epidote, diopside, garnet and a wide spectrum of sulphide minerals. There are indications of two phases of hydrothermal ores in the rock body, an earlier phase with disseminated ores, can be distinguished form a younger formation of veins with massive sulphide infillings.

In the earlier phase, minor amounts of pyrite, and sphalerite grew sporadically in the veins. FINTOR et al. (2009) determined a Ca-Al silicate dominant mineral assemblage with a di → ep ± czo →sp → ab ± kfs → chl → adu → prh → py → cal mineral sequence (mineral abbreviations after SIIVOLA & SCHMID (2007), Table I., except for adularia: adu). A detailed geochemical and fluid inclusion investigation of the vein filling minerals indicates that mineral precipitation occurred during cooling of the hydrothermal system. The *T-X* character of the fluid changed from high temperature (467–370 °C) and low salinity (0.2–1.5 mass% eq. NaCl) down to lower temperature (~150 °C) and low- to moderate salinity (3–6 mass% eq. NaCl) appear in fluid inclusions of diopside, epidote, and calcite phases (FINTOR et al., 2009). Chlorite thermometry data (300 → 140 °C) also supports decreasing temperatures during the vein filling process. Many of these studied veins are surrounded by 0.5–2 cm thick alteration halos.

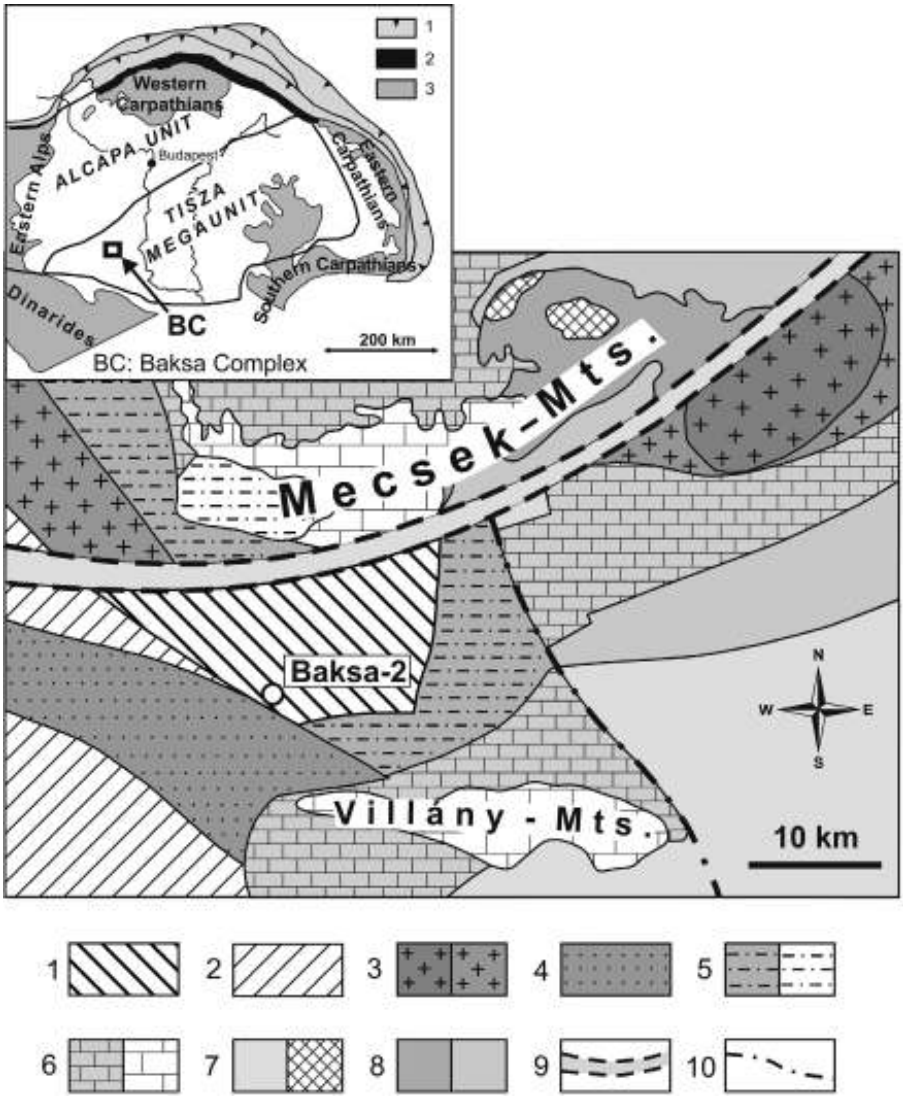

Figure 1: The geological map of the Baksa Complex and its environs is presented without Tertiary and Quaternary sediments. Legend: 1. Baksa Complex (study area), 2. Babócsa Complex, 3. Mórágy Complex (Carboniferous), 4. Carboniferous sediments, 5. Permian formations, 6. Triassic formations, 7. Jurassic formations, 8. Cretaceous formations, 9. Mecsekalja Tectonic Zone,, 10. Villány-Szalatnak deep fracture zone. Inset: Location of the study area (BC) in the Pannonian Basin (ALCAPA and Tisza mega unit are also represented on the map); Inset legend: 1. Flysch Belt, 2. Pieniny Klippen Belt, 3. Inner Carpathian Mountain Belt.

A detailed investigation of mineralogy and ore genesis of the veins with massive sulphide ore infillings was carried out by TARNAI (1997, 1998). In a study of fluid inclusions of the quartz which was cogenetic with the later ore minerals, he determined a trapping temperature (T_t), of 240 to 300 °C and trapping pressure (p_t), of 15–30 MPa (TARNAI, 1998). The youngest alteration phase that can be investigated in the rocks is a retrograde greenschist facies event, which caused chloritization and secondary albitization (SZEDERKÉNYI, 1979). Its temperature range is assumed to be 200–400 °C by ÁRKAI et al. (1985). The beginning of this event is related to the Alpine orogeny (SZEDERKÉNYI, 1984). FINTOR et al. (2008) detected traces of high salinity fluids (~20–25 mass% eq. NaCl) in the post-metamorphic quartz-carbonate veins that penetrate the rock body. Using microthermometry, they obtained conditions of approximately 80–180 °C and 20–100 MPa for the formation parameters of the quartz-carbonate veins.

The Baksa-2 exploratory well (bottom-hole: 1200 m) enables the most detailed investigation of the BC (Fig. 2). It exposes the crystalline basement formation with a total thickness of over 1100 m and near 100% core recovery. The metamorphic mass was divided (SZEDERKÉNYI, 1979) into the following lithostratigraphic units:

Upper marble section (57–224 m)
Chloritic two-mica gneiss (224–822 m)
Lower marble section (822–867 m)
Garnetiferous two-mica gneiss (867–922 m)
Garnetiferous two-mica schist (922–1200 m)

Upper marble section

Marble and dolomite marble are the predominant rock types in this section with gneiss and mica-schist intercalations. Aplite dykes frequently occur in the section and significant alterations in carbonate rocks can be related to them. These alterations are accompanied by the formation of calc-silicate hornfels with epidote and diopside. Ore showings caused by hydrothermal fluids are also common. The most significant ore vein (6–7 cm thick) is found at 186.4 m depth. The formation conditions and ore mineral paragenesis (pyrite, pyrrhotite, sphalerite, chalcopyrite, galena, pentlandite, hematite, covellite, marcasite) of the vein were investigated in detail by TARNAI (1997; 1998); who assumed that these veins were formed in relation to the rhyolitic volcanism that occurred near the northern margin of the Villány Mountains (FAZEKAS & VINCZE, 1991).

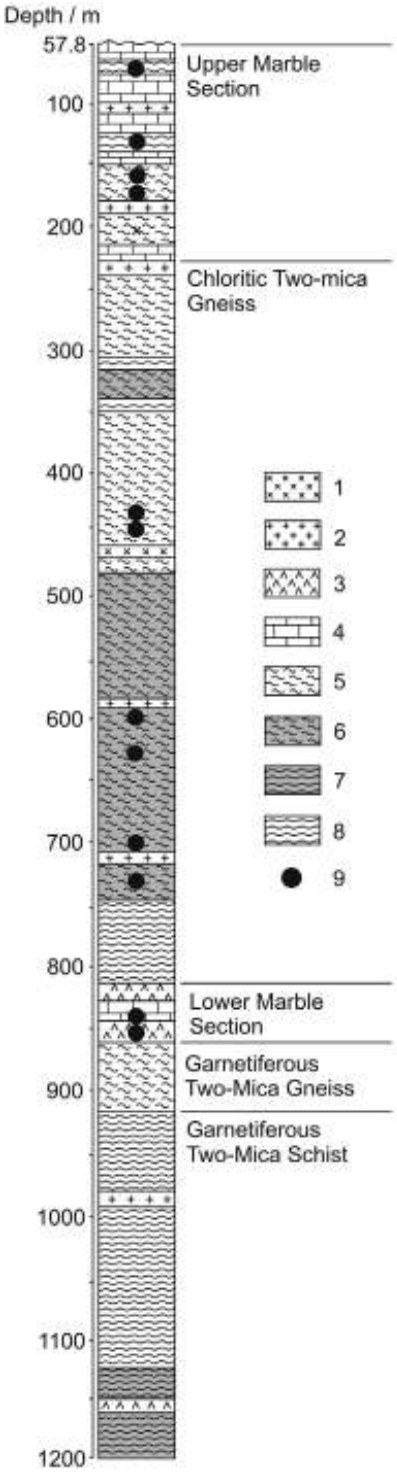

Figure 2: Lithological profile of the Baksa-2 borehole. (after SZEDERKÉNYI, 1979) Legend: 1. Biotite-andesite dyke 2. Aplite dykes 3. Amphibolite 4. Marble and Dolomite marble 5. Two-mica gneiss 6. Chloritic gneiss 7. Chloritic schist 8. Two-mica schist 9. Sampling points.

Chloritic two-mica gneiss

This section is composed of two-mica gneiss and schist with some amphibolite. Significant chloritization (after biotite) is observed in some parts of the rocks (SZEDERKÉNYI, 1979). Aplite dykes are rare in this section and a cross-cutting biotite-andesite dyke is observed in a fault zone at approximately 460 m depth.

Lower marble section

This section is comprised of amphibolites, although marble intercalations are the most important rock type of the section. The marble bands are almost pure dolomite. This section is very rich in aplite dykes, which caused alterations similar to those found in the upper marble section.

Garnetiferous two-mica gneiss

This rock section is dominated by gneiss with some mica schist intercalations. Large garnet grains (> 2 cm in diameter) are a common occurrence throughout the section. Aplite dykes do not occur in this section.

Garnetiferous two-mica schist

This section consists predominantly of mica schist, with lesser amounts of gneiss and some amphibolite. Garnets with similar characteristics to those of the garnetiferous two-mica gneiss also occur in considerable amounts. One aplite dyke was discovered in the section, which suffered comprehensive epidotization and tourmalinization.

3. SAMPLES AND METHODS

Samples used for analysis were collected throughout the profile of the Baksa-2 drillhole, as detailed locations on Fig. 2 show. Mineral abbreviations used in the whole study (Table I) are after SIIVOLA & SCHMID (2007).

X-ray element maps and bulk rock chemical analyses were made using a Horiba Jobin Yvon XGT 5000 X-ray fluorescence spectrometer. Beam diameter was 100 μm and acceleration voltage was 30 kV in each case. Bulk analyses were made from 5 mm x 5 mm areas of rock surfaces. Analyzed areas were divided into 512 x 512 pixels with 0.01 mm^2 size of each pixel. Natural standards were used for standardization of each measured element. The Surfer 8 surface mapping system was used for the representation of element maps obtained by XRF analyses.

Isocon analysis was made from bulk rock chemical data using the computer program GEOISO (COELHO, 2006). This program can calculate and plot (Isocon diagram), the mass and volume changes that can occur in a wide variety of open system geological processes. The Isocon diagram is based on the study of GRANT (1986, 2005) and is a simple solution to GRESENS (1967) equation for metasomatic alteration.

Gresens' basic argument is that some components are likely to have been immobile during the alteration process, and if these can be identified, they can be used to establish any change in volume which has taken place. Gains or losses of other components can then be calculated, assuming that the volume change is a factor common to the behaviour of all components. GRESENS (1967) shows that the transformation of a generic rock A into another generic rock B can be expressed as follows:

$$X_n = [f_v(g^B / g^A)\, C_n^B - C_n^A]\, a$$

Table I: Summarized list of abbreviations of minerals used (after SIIVOLA & SCHMID, 2007).

Mineral	Abbreviation
albite	*ab*
adularia	*adu*
biotite	*bio*
calcite	*cal*
chalcopyrite	*ccp*
chlorite	*chl*
clinozoisite	*czo*
diopside	*di*
epidote	*ep*
galena	*gn*
hematite	*hem*
K-feldspar	*kfs*
muscovite	*mu*
pentlandite	*pn*
pyrite	*py*
pyrrhotite	*po*
prehnite	*prh*
rutile	*rt*
sericite	*ser*
sphalerite	*sp*
titanite	*ttn*

where "X" is the mass change of component "n" relative to "a", "n" the considered component, "g" the densities of each rock, "v" the volume of each rock, "f_v" a volume factor, "a" the mass of the original sample (A) and "C" the concentration.

Even if efficient, the Gresens' method is neither easy nor practical to use. GRANT (1986) proposed a more direct and easier process of using Gresens' equation in the following expression:

$$C_i^f = (M^0 / M^f)(C_i^0 + \Delta C_i)$$

where "C_i^f" is the resulting concentration of component "i", "M^o" is the mass of the original, while "M^f" is the mass of the transformed rock, "C_i^0" is the original concentration of component "i" while "ΔC_i" is the change of concentration of component "i".

For each component there is an equation of this form, in which (M^o/M^f) is constant. The "perfectly inert" elements must define a line $C_i^f = f(C_i^0)$, of slope M^o/M^f passing through the graph origin. The line connecting "points with the same concentration", GARY et al. (1974), is defined as an "isocon". Using the computer software GEOISO, the whole rock mass change (M^f-M^o/M^o) and volume change (V^f-V^o/V^o) are also calculable. The program estimates the element mass changes during alteration using two different approaches. In one case the program compares each elements mass change to the original rock mass:

$$(M_i^f - M_i^0)\, M^0 = (M^f / M^0)\, M_i^f - C_i^0$$

where M_i^f is the mass of component "i" in the transformed rock, and M_i^0 is the mass of component "i" in the original rock. Alternativley, the program compares each elements mass change to its mass in the original sample:

$$(M_i^f - M_i^0)\, M_i^0 = (M^f / M^0)\, C_i^f / C_i^0 - 1$$

Given the better approach, the latter equation was used in this study to estimate element mass changes. In our study we use the nomenclature and abbreviations by GRANT (1986).

Densities of the different metasomatic zones were calculated using the *THERIAK* (HOLLAND & POWELL, 1998; DE CAPITANI, 1994; DE CAPITANI & BROWN, 1987) thermodynamic program package.

Fluid inclusions were studied in 75–150 μm double-polished thick sections prepared from the vein filling minerals. Microthermometric measurements were carried out by means of a Linkam THMSG 600 heating-freezing stage, operating over a temperature range from –190 to 600 °C. Synthetic fluid inclusions were used to calibrate at –56.6, 0.0 and 374.0 °C. The accuracy of the data is ±0.2 °C under freezing and ±0.5 °C under heating conditions. An Olympus LMPlanFI 100X objective was used to analyze the inclusions. The cycling method (GOLDSTEIN & REYNOLDS, 1994) was used to determine the last ice melting temperatures, and each melting of ice occurred in the presence of a vapour phase. Estimations of volume fractions of vapour bubbles ($\varphi_{vap}=V_{vap}/V_{liq+vap}$) were obtained from area analysis of a two-dimensional projection of the fluid inclusions. Terms and symbols of DIAMOND (2003) were used.

The computer package *FLUIDS* (BAKKER 2003) was used to calculate fluid properties. The program *AqSo2e* was used to calculate salinities in the NaCl-H_2O systems (NADEN, 1996) based on the equivalent mass % principle. The program *BULK* (BAKKER, 2003) allowed us to calculate the bulk fluid properties molar volume (V_m), and bulk composition of individual fluid inclusions. This calculation was accomplished using a purely empirical thermodynamic model, the equation of state for electrolyte-bearing aqueous solutions of KRUMGALZ et al. (1996) and the volume fractions of the liquid phase of the inclusions at room temperature.

A Jobin Yvon LABRAM confocal Raman spectrometer, equipped with a frequency doubled Nd-YAG laser (100 mW, 532.2 nm), with a 100X/0.80 objective lens was used to identify fluid phases in inclusions. The spectrometer was calibrated using a silicon chip. The spectral resolution of the instruments was 4 cm^{-1} and the spatial resolution was a few μm^3. The acquisition time was 100 s with 20 s accumulation periods in each spectrum.

4. RESULTS

4.1. Petrography and Mineralogy

In many parts of the metapelitic (gneiss, mica schist) section of the BC, significant wall-rock alteration is observable along Ca-Al silicate veins (Figs. 3A, B). These alterations appear as symmetrical narrow (up to few cm thick) bleached

margins beside thin veins and broad alteration bands along thick veins where epidotization and chloritization of the adjacent rock are recognizable. The following mineralogical characteristics were observed from the veins toward the unaltered wall rocks.

Very close to the vein wall (in a 2–5 mm thick band) the feldspar porphyroblasts (albite) exhibit a turbid appearance because of micro-sized pores (<2 μm fluid inclusions), that fill the entire grain (Fig. 4A, C). The micas (muscovite+biotite) of the unaltered wall rock found among feldspar porphyroblasts are totally replaced by albite. These albite pseudomorphs form elongated grains with irregular grain boundaries (Fig. 4A) and frequently contain tiny euhedral titanite inclusions (Fig. 4B). In both the albite pseudomorphs and in the albite porphyroblasts, small (<0.5 mm) cavities occur in significant amounts. Euhedral albite crystals have frequently

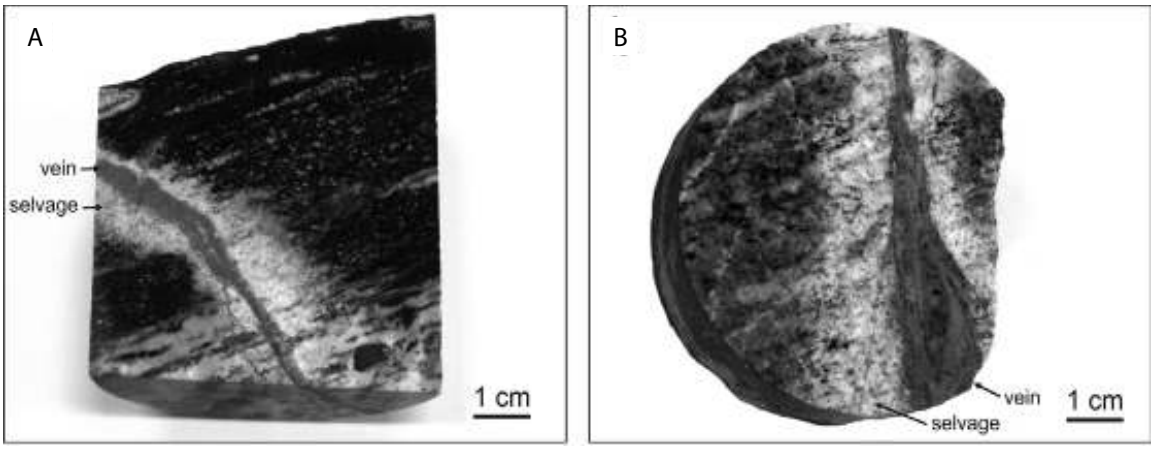

Figure 3: Typical symmetrical wall-rock alteration patterns along propylitic veins. A) Symmetrical bleached margin along $V_{cpx\text{-}ep}$ vein (wall-rock: biotite gneiss); B) symmetrical bleached margin along $V_{ep\text{-}chl}$ vein (wall-rock: chloritic two-mica gneiss)

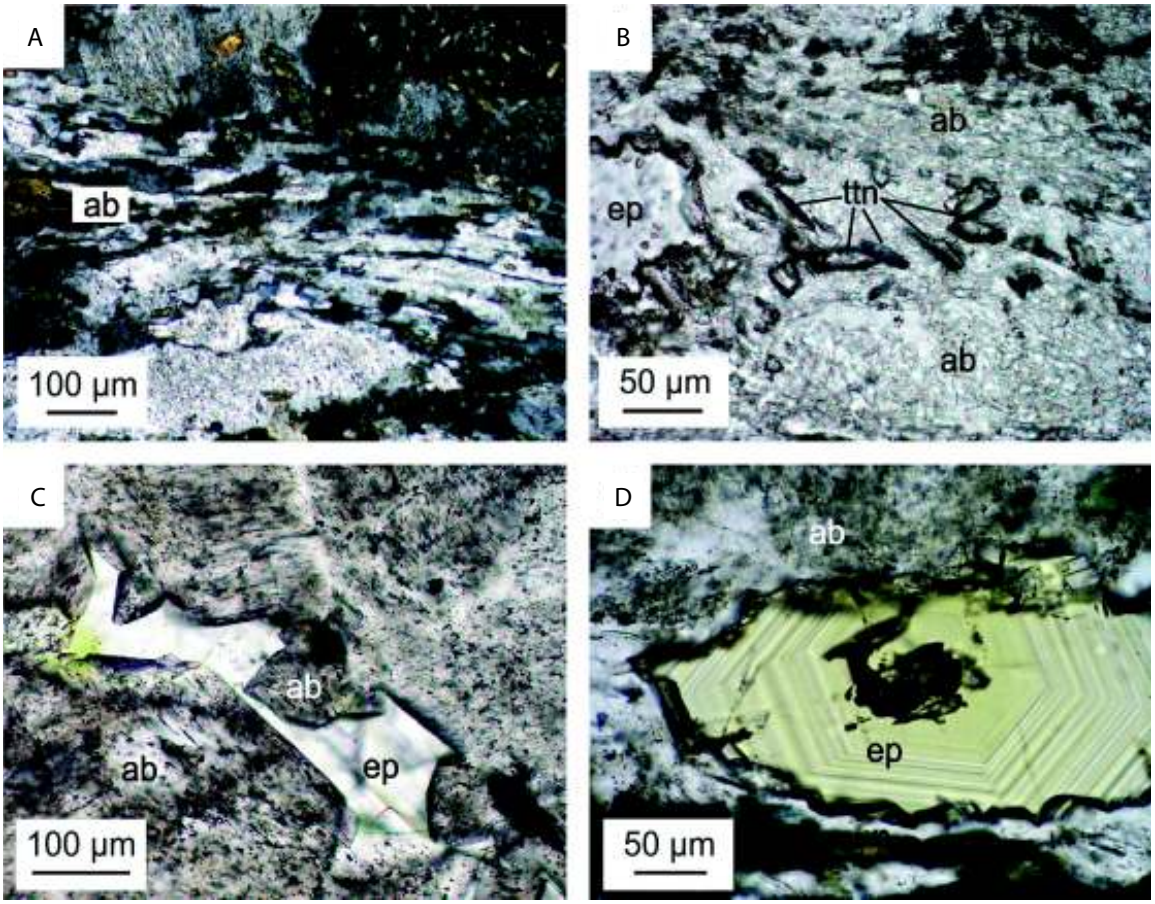

Figure 4: Alteration mineral assemblages in the margin closest to the veins. A) Irregularly bordered elongated albite pseudomorph after mica (+N); B) group of euhedral titanite inclusions in an albite pseudomorph (1N); C) euhedral albite crystal growth in a cavity filled by epidote, (note the many micro pores in albite) (1N); D) well developed growing zonation in a cavity filling epidote crystal (1N)

grown on the walls of the cavities (Fig. 4C). The cavities are filled with epidote that often shows a characteristic zoned growth pattern (Fig. 4D). The alteration mineral paragenesis of this domain is: *ab + ttn±ep*

Towards the wall rock the amount of albite pseudomorphs after micas markedly decreases. The amounts of micropores observable in the albite porphyroblasts also gradually decreases. Small patches of sericite inclusions appear in the feldspar crystals and their amount progressively increases towards the wall-rock. Epidote and chlorite replacement after biotite become dominant in the altered domains of the wall-rock (Fig. 5A–F). Well developed epidote and chlorite pseudomorphs occur in the formerly mica rich bands (Fig. 5A). Among the epidote and chlorite pseudomorphs, euhedral titanite crystals frequently occur (Fig. 5B). Elongated cavities in the strongly epdotized metapelites, are sometimes filled by very fine grained epidote (Fig. 5C). Nevertheless epidote occurs as hypidiomorphic inclusions in chlorite along the cleavage (Fig. 5D). In some places, anhedral epidote aggregates "float" in a chlorite rich matrix (Fig. 5E) together

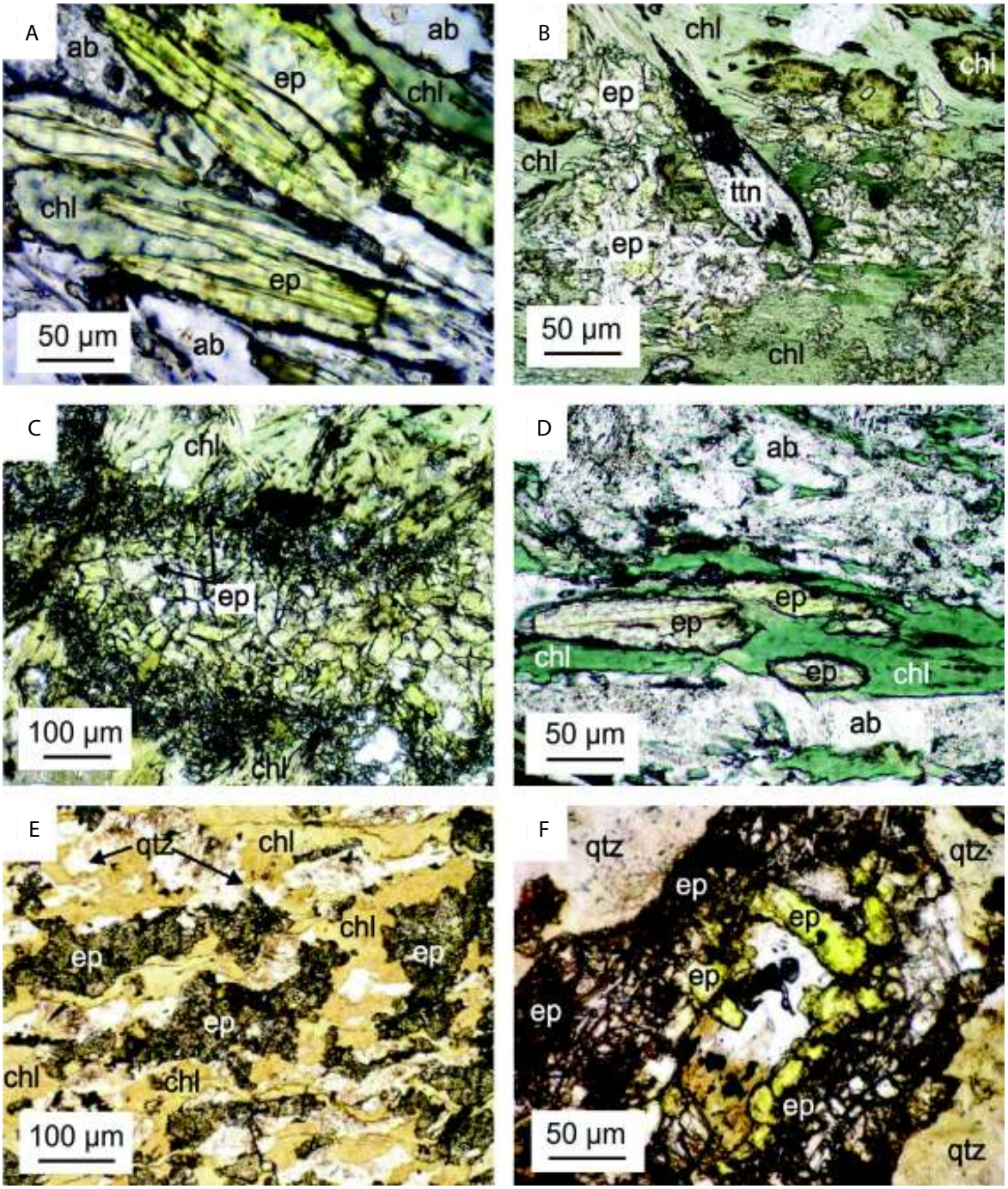

Figure 5: Alteration mineral assemblages from the most epidotized and chloritized parts of the margin. A) epidote and chlorite pseudomorphs after biotite (+N); B) euhedral titanite crystal among a mass of replacement epidote and chlorite (1N); C) elongated cavities filled by fine grained epidote crystals in a chlorite matrix (1N); D) epidote pseudomorphs as inclusions in chlorite replacing biotite (1N); E) fine grained anhedral epidote aggregates among chlorite and quartz rich bands along schistosity (1N); F) subhedral elongated epidote crystals among fine grained anhedral epidote (1N)

with anhedral fusiform quartz grains. Here, epidote shows strongly dissolved surfaces and is composed of very fine epidote grains (Fig. 5F). Among the little grains, elongated hypidiomorphic, almost clear epidote crystals are observable (Fig. 5F). The alteration mineral paragenesis is: *ep + chl + ttn + ab ± ser.*

Towards the unaltered wall-rock, the amount of epidote replacing biotite decreases and chloritization of biotite becomes characteristic. Furthermore, increasing numbers of biotite relics can be observed in the chloritized domains (Figs. 6A, B). Titanite is almost totally absent from this area, but acicular sagenite rutile inclusions can occasionally be observed in the chlorite pseudomorphs (Fig. 6C). Muscovite does not show any alteration except for minor sericitic recrystallization at some places. The alteration mineral paragenesis is: *chl + ep + ser + rt ± ttn.*

In the unaltered wall rock part of the alteration zones, sericite is the major alteration mineral. It occurs as tiny lamellar inclusions in feldspars, and frequently forms sericitic rims around the clear cores of feldspar grains (Fig. 6D). Micas show a fresh appearance except for partially chloritized biotite flakes. Epidote occurs only as a cavity filling mineral phase, which frequently occurs, even in the unaltered wall-rock far from alteration zones. Alteration mineral paragenesis in this domain is: *ser ± chl.*

4.2. Element maps and bulk rock chemistry

Element distribution maps were made from the veins and their adjacent environments including alteration halos and unaltered wall-rocks of gneiss and mica schist (Fig. 7). The results show that characteristic element distribution patterns can be observed along the studied veins. Based on X-ray maps, the most characteristic distribution patterns can be observed in the case of Si, Fe, Ca, K, and Ti in the veins and their immediate environments (Fig. 7). Bulk rock analyses made from domains show individual alteration parageneses. Results are summarized in Table II where the numbers in brackets (1 to 4) on the head of the columns refer to the different domains (show individual mineral parageneses), from vein to wall rock. The results of bulk rock chemical analyses (Table II) support the estimations from element maps. Besides the obvious differences between margins and unaltered wall-rock, with regard to their composition (*wt* %), the rock density data show that the bulk rock density markedly increases from the veins toward the adjacent rocks (Table II).

4.3. Fluid inclusion petrography and microthermometry

Analyses were made of fluid inclusions from cavity filling epidote (Fig. 4D) and elongated epidote crystals that occur

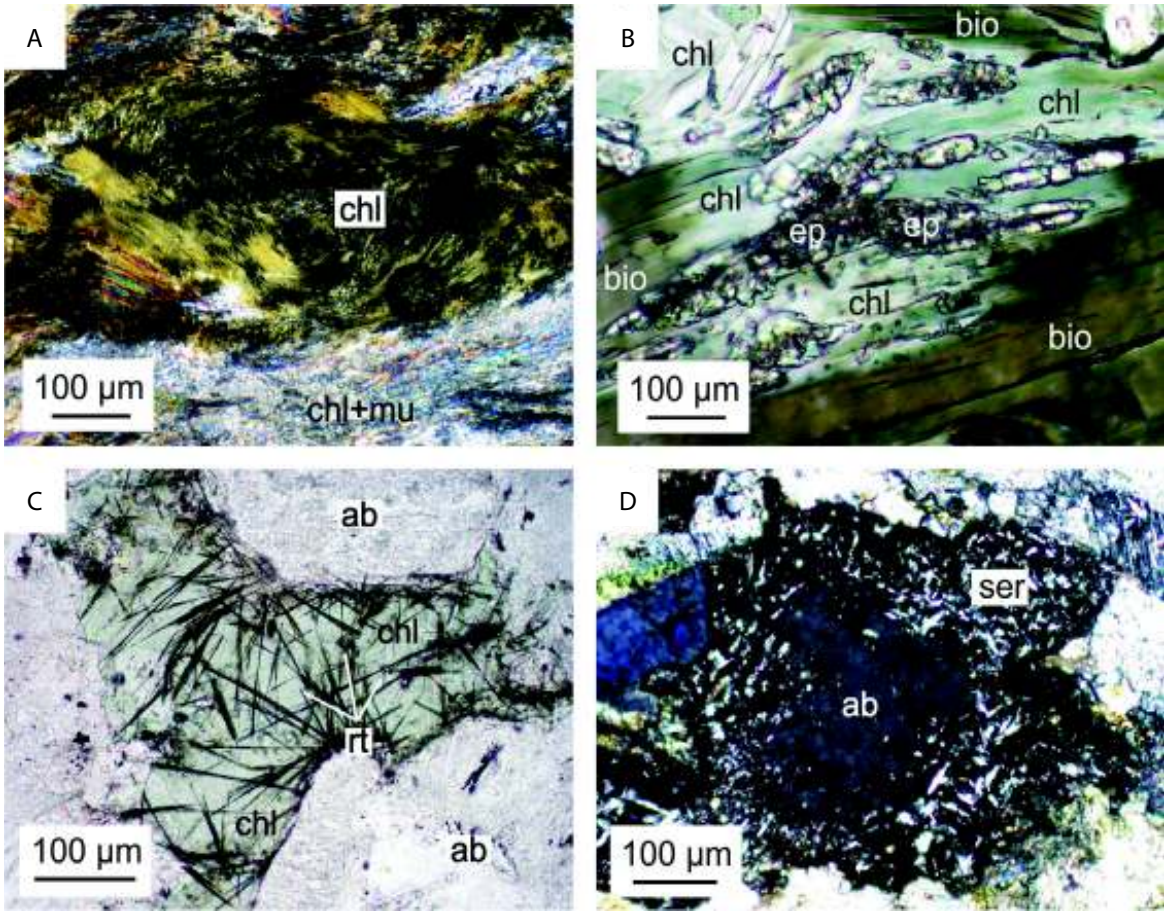

Figure 6: Alteration mineral assemblages in the margin closest to the unaltered wall-rock. A) Chlorite rich band with muscovite in the strongly chloritized domains (+N); B) chloritization and epidotization of biotite (1N); C) acicular rutile inclusions in chlorite pseudomorph after biotite (1N); D) sericitization of feldspar, albite crystal core with a well developed sericite crown (+N)

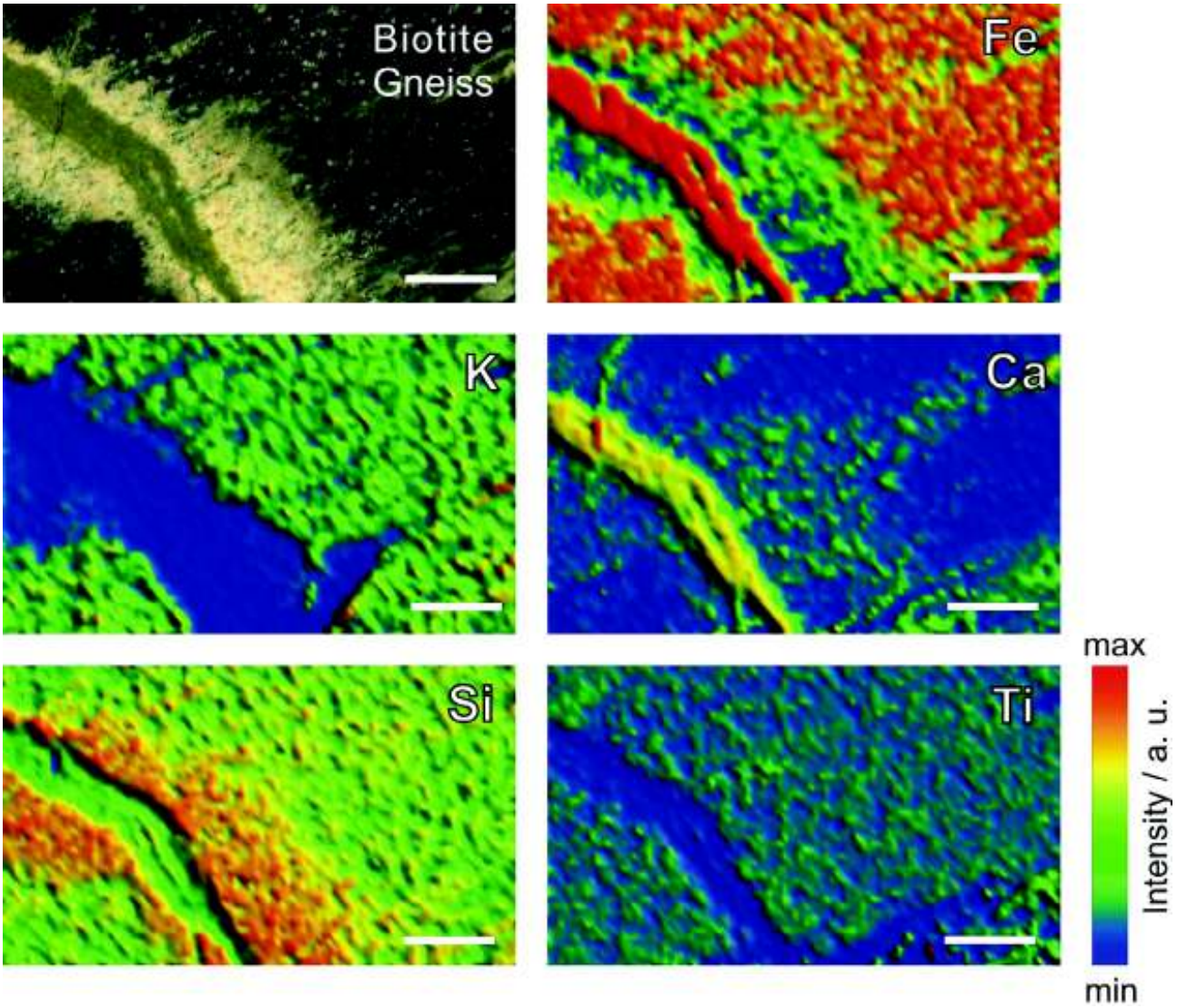

Figure 7: X-ray element maps about a vein with characteristic symmetrical margins (3D surfaces were constructed by Surfer 8), where relief and colour intensity represent the relative concentration of the different elements. Bar scale is 1 cm.

Table II: Whole rock chemical data from the margins and the unaltered wall-rock. Numbers 1 to 4 in brackets at the head of the columns refer to domains characterized by individual alteration mineral paragenesis. Legend: (1) *ab+ttn±ep*; (2): *ep + chl + ttn + ab ± ser*; (3): *chl + ep + ser + rt ± ttn*; (4): *ser ± chl*, abbreviation UA refer to unaltered.

Oxides (wt%)	**637** (1)	**637** (2)	**637** (3)	**637** (4)	**637 UA** (average of 4 measurements)
SiO_2	68.81	63.53	64.80	60.59	60.59
TiO_2	0.95	0.88	0.85	0.91	0.88
Al_2O_3	17.65	18.09	19.19	19.05	19.07
Fe_2O_3	1.15	1.48	2.10	5.47	7.21
MnO_2	0.13	0.15	0.17	0.23	0.37
MgO	0.00	0.26	0.78	1.33	1.09
CaO	4.25	4.09	3.84	4.07	2.10
Na_2O	6.07	8.99	4.63	5.43	5.23
K_2O	0.31	1.72	2.98	2.27	2.70
P_2O_5	0.43	0.57	0.41	0.38	0.56
Total	99.75	99.75	99.76	99.74	99.78
Density (g/cm^3)	2.67	2.65	2.72	2.76	2.77

among fine grained epidote aggregates (Fig. 5F). The four selected samples originated from 80.6 m, 436.2 m, 730 m, and 858.8 m depths in the drillhole.

In cavity filling epidote grains (Fig. 8A), four types of fluid inclusion assemblages (FIA) can be distinguished based on fluid inclusion petrography.

A group of fluid inclusions composed of solitary two phase (L+V) liquid dominant fluid inclusions occur randomly, or in small clusters in the host crystals (Figs. 8B, C). Their longest dimension is 5–10 μm. They are not related to growth zones of the host mineral and can not be found along cleavage planes or microcracks. Definitive evidence for their primary origin is the occurrence of fluid inclusions along growth zones (GOLDSTEIN & REYNOLDS, 1994; BODNAR, 2003). Less conclusive is the occurrence of one, or a few inclusions, in the interiors of the minerals (BODNAR, 2003) as is the case for the aforementioned group of inclusions. These inclusions are considered to be primary based on their distribution within the crystal (BODNAR, 2003). Based on phase volume ratios, two primary FIAs, a P1 with

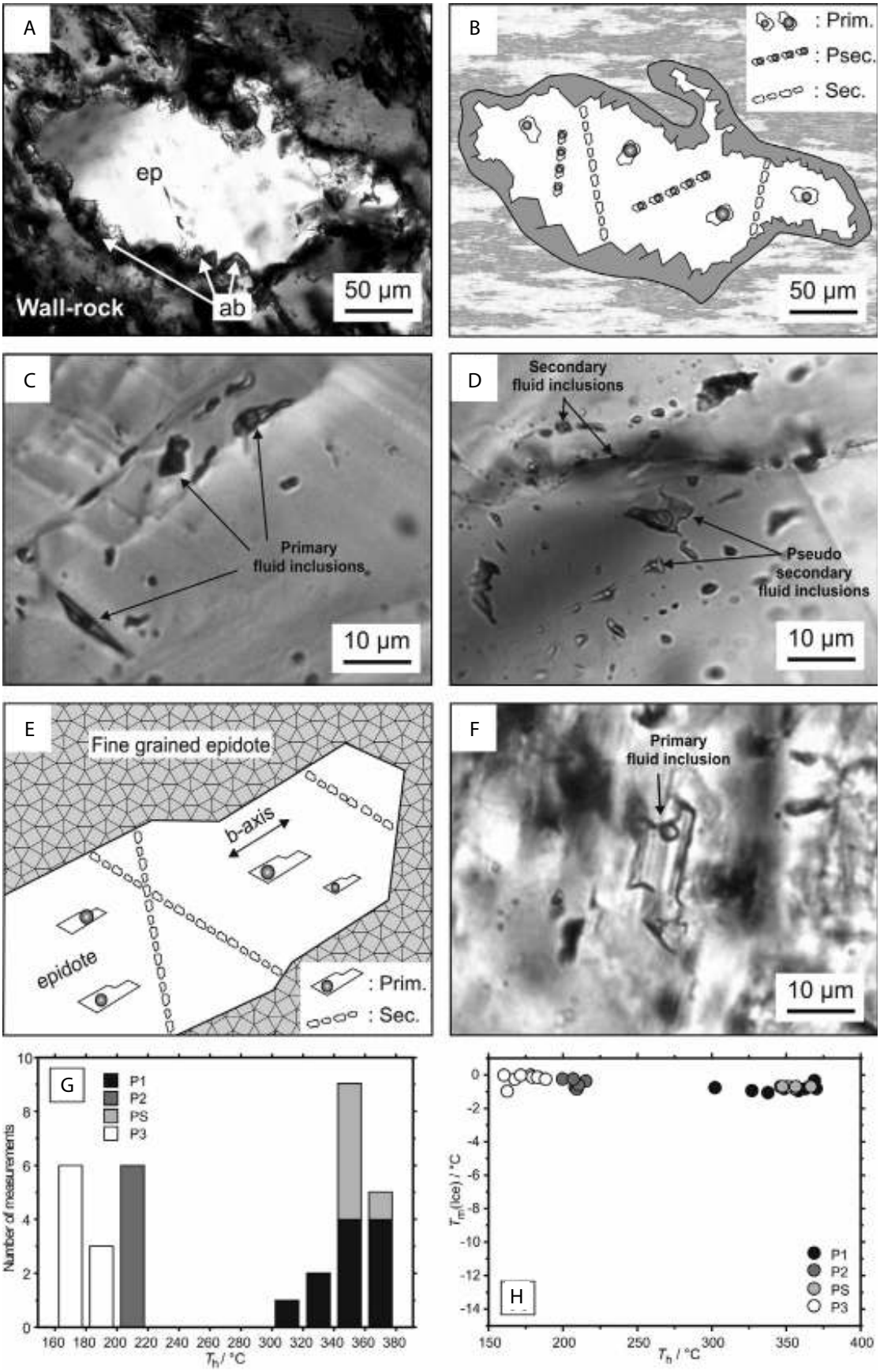

Figure 8: Results of fluid inclusion studies: A) cavity filled by epidote and euhedral albite crystallised cloase to the cavity wall (+N); B) schematic sketch of the distribution of different fluid inclusion assemblages in the cavity filling epidote; C) primary fluid inclusion assemblage in a cavity filling epidote (1N); D) pseudo secondary fluid inclusion assemblage in cavity filling epidote (1N); E) schematic sketch of the appearance and distribution of different FIA in the subhedral epidote grains that can be found among fine grained epidote; F) primary fluid inclusion in subhedral elongated epidote grain (1N); G) histograms of T_h values of each FIA; H) T_h vs T_m(Ice) plot of each investigated FIA.

higher (φ_{vap}= 0.3–0.45) and a P2 with lower (φ_{vap}~ 0.15) degree of filling values were distinguished (Table III), although their relative ages cannot be determined. Fluid inclusions of both assemblages contain an aqueous electrolyte solution without any detectable volatile content based on Raman data. Because eutectic melting (T_e) could not be determined in the inclusions, the chemical composition was not ascertainable. Salinity is expressed using the mass% eq. principle (NADEN, 1996). In the P1 assemblage the T_m(Ice) values are very similar; all measured values are between –1 and –0.4 °C (n=10) (Fig. 8H; Table III) indicates low salinity (0.4–1.6 mass% eq. NaCl) (Table III). Homogenization temperatures are within the 303–364 °C (n=10) range (Fig. 8G, H; Table III). In the P2 FIA the T_m(Ice) values vary between –0.8 and –0.3 °C (n=6) (Fig. 8H; Table III) indicating low salinity between 0.2 and 1.2 mass% eq. NaCl, while T_h values occur in a narrow range between 201 and 214 °C (n=6) (Fig. 8G, H; Table III).

Fluid inclusions also occur along planes that do not reach the grain boundary of the host crystals (Fig. 8B). Their longest dimension is 5–10 µm containing liquid and vapour phases (L+V), and show a liquid dominant (φ_{vap}= 0.4–0.45) character (Table III). We regard these inclusions as pseudosecondary (PS) based on criteria after BODNAR (2003). In the PS assemblage the T_m(Ice) values have a very narrow range around –0.8 °C (n=6; salinity: ~ 1 m% eq. NaCl; Fig. 8H; Table III), while T_h values are between 344 and 361 °C (n=6) (Figs. 8G, H; Table III).

Healed microcracks can be found in some parts of the host epidote, and these cracks run through the whole grains (Fig. 8B). Fluid inclusions occurring along these healed cracks are very small (less than 3µm), they contain one phase liquid (φ_{vap} ~ 0) (Table III) and are definitely secondary in origin. They are not appropriate for microthermometry.

In the elongated epidote crystals that occur in the fine grained epidote matrix (Fig. 5F.), two fluid inclusion assemblages can be observed (Fig. 8E). Two phase (L+V) liquid dominant (φ_{vap} ~0.1) aqueous inclusions, with elongated shapes (Fig. 8F; Table III) can be found in the crystals. Their longest dimensions are in the 5–15 µm range, and although they are not concentrated in a particular growth zone, their elongation in the direction of crystallographic b-axis of epidote (Fig. 8E) indicates formation during crystal growth (KLEMD, 2004). Based on these considerations, the inclusions are most probably primary in origin and denominated as P3. The measured T_m(Ice) values of fluid inclusions of P3 are between –0.1 and –0.9 °C (n=9) (Fig. 8H; Table III) indicating a low salinity fluid (0.2–1.4 mass% eq. NaCl; Table III). The homogenization temperatures are in the 163–186 °C (n=9) interval (Figs. 8G, H; Table III).

Small (<3 µm), aqueous one phase (L), irregularly shaped inclusions can be found along trails which crosscut the entire crystals. These inclusions are secondary ones (S) in origin (Table III). They occur in subordinate amounts and they are inappropriate for microthermometry.

5. DISCUSSION

5.1 Metasomatism of the wall-rock

The occurrence of the same modification of wall-rock from narrow symmetrical margins along thin veins to wider altered domains is observable. Different types of wall rock alterations along veins have been studied in detail by many researchers (SCHERBAN, 1996; OMEL'YANENKO, 1978; SCHERBAN, 1975; KORZHINSKII, 1946). Occurrence of symmetrical alteration rims around veins is typical feature of so called "near vein metasomatism" (ZHARIKOV et al., 2007).

Metasomatic zones (ZHARIKOV et al., 2007) are denominated as zone 1 to zone 4 (zone 1 represents the closest and zone 4 the farthest domain from the vein), and can be assigned on the basis of the individual mineral paragenesis of the altered domains. The metasomatic column (metasomatic facies) (ZHARIKOV et al., 2007) is built up by the following zones:

Zone 1: In this zone albite and titanite are the most characteristic minerals, mineral paragenesis*: ab + ttn ± ep.*

Zone 2: Here, the appearance of epidote pseudomorphs after biotite flakes is the most characteristic alteration feature. Mineral paragenesis is *ep + chl+ ttn + ab ± ser.*

Zone 3: The amount of epidote markedly decreases and the chlorite content increases. Sericite is more common and rutile inclusions in chlorite frequently occur. The mineral paragenesis is *chl + ep + ser + rt ± ttn.*

Zone 4: Sericitization is the most characteristic alteration process in this zone; other alteration minerals are in subordinate amounts. The mineral paragenesis consists of *ser ± chl.*

Whole rock chemical changes during metasomatic alteration of the wall-rock to alteration halos were evaluated by GRANT'S (1986) method using the whole rock chemical

Table III: Summary of the results of the fluid inclusion study.

Host mineral	Type	Number of Inclusions	Phases (25 °C)	φ_v	T_h (°C) V→L	T_m(Ice) (°C)	Salinity NaCl eq. mass %
Cavity filling epidote	P1	10	L+V	0.3–0.45	303–364	–0.7±0.3	0.4–1.6
	PS	6	L+V	0.4–0.45	344–361	~–0.8	~1
	P2	6	L+V	~0.15	201–214	–0.55±0.25	0.2–1.2
	S	–	L	–	–	–	–
Elongated epidote crystals	P3	9	L+V	~0.1	163–186	–0.5±0.4	0.2–1.4
	S	–	L	–	–	–	–

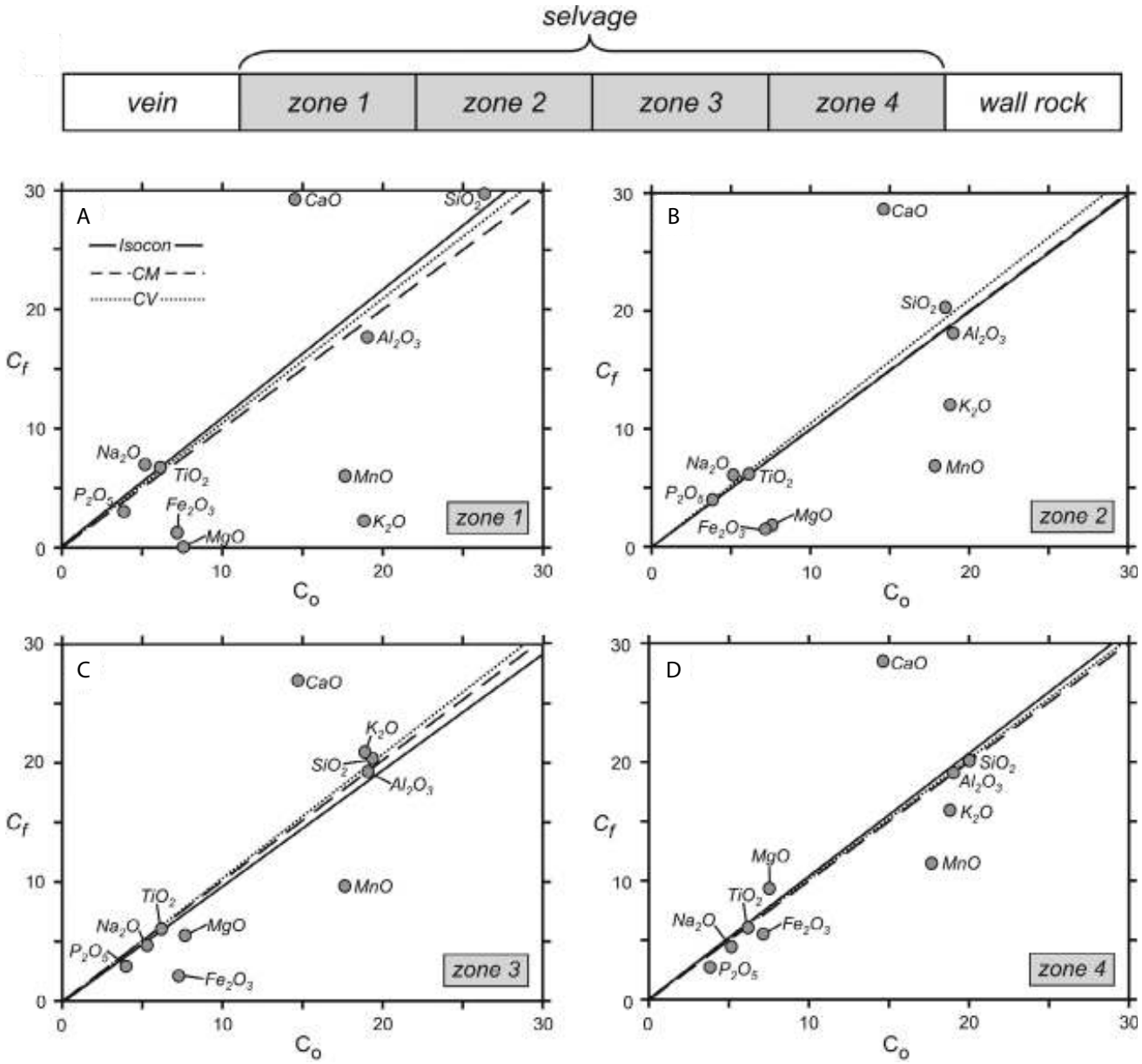

Figure 9: Isocon diagrams of an altered domain occur along propylitic veins. where C_o refers to the concentration before, while C_f refers to the concentration after alteration. A) isocon diagram of metasomatic zone 1; B) isocon diagram of metasomatic zone 2; C) isocon diagram of metasomatic zone 3; D) isocon diagram of metasomatic zone 4. CM (dashed line) indicates constant mass-, while CV (dotted line) the constant volume line on the diagrams.

data (Table II). Isocon diagrams were constructed to compare the alteration halo with the unaltered wall-rock. Isocon analyses were undertaken using whole rock chemical data of the different metasomatic zones detailed above. This procedure resulted in four isocon diagrams labelled from zone 1 to zone 4 (Fig. 9A.). In order to define the best fit isocon, TiO_2 was used as an inert constituent for each isocon diagram. Titanium can be found in the altered domains as titanite and/or rutile in the pseudomorphs after biotite flakes, indicating that the Ti content of the wall rock was not changed during the alteration process (Fig. 7*;* Table II). The most obvious characteristics of each isocon diagram are the significant gain of CaO in the alteration halo relative to the wall-rock. The amount of the gain is almost identical from the vein to the unaltered wall-rock (Figs. 9B, C, D, E). The contents of SiO_2, Al_2O_3, Na_2O and P_2O_5 behave very conservatively. They do not show any significant change except for a minor gain of SiO_2 (Figs. 9B, C, D) and Na_2O close to the vein (Fig. 9B) and a minor loss of Al_2O_3 (Fig. 9B). Characteristic losses can be detected in concentrations of Fe_2O_3, MgO, MnO, and K_2O. The Fe_2O_3 and MnO behave similarly; their concentrations decrease gradually from wall-rock towards the vein, except closest to the wall rock where minor differences are observable. (Fig. 9B, C, D, E). The MgO content shows an intensive decrease towards the vein and only a little gain closest to the wall-rock. Significant loss of K_2O can be observed in the alteration halo (Fig. 9B, C, E), but a minor gain is detectable close to the unaltered wall-rock (Fig. 9D).

Comparison of the results of the textural observations and isocon analyses may contribute to a better understanding of those processes that induced the characterized alteration patterns in the Baksa gneisses.

The most significant alteration that occurs in great abundance from narrow margins along thin veins to massive alterations of wall-rocks, are epidotization and chloritization of biotite. In some places, albite replacement after micas is also characteristic. In order to better explain the alteration processes, we present the most significant element mass changes as a function of the original mass (Fig. 10). Here, the relative mass changes of elements $(M_i^f\text{-}M_i^o)/M_i^o$ are represented as a function of distance from propylitic veins.

In the immediate few mm of the veins (Fig. 10, zone 1), micas (muscovite+biotite) are totally or partially replaced by albite (Fig. 4A). This phenomenon is most probably due to hydrothermal leaching that almost totally removed K, Fe, Mn, and Mg, from these areas (Figs. 9B, 10/zone 1). Simultaneous to the decomposition of micas, albite crystals of the wall-rock were dissolved by the fluid and were recrystallised in place of the micas. Using known compositions of reagent minerals (ÁRKAI et al., 1999; FINTOR, 2005) a relevant reaction equation (1) can be formulated based on constant Al:

$$\underset{\text{muscovite}}{K_{1.7}Na_{0.3}Mg_{0.12}Fe_{0.1}Al_{3.7}\left(Al_{1.8}Ti_{0.06}Si_{6.2}O_{20}\right)(OH)_4} +$$

$$\underset{\text{biotite}}{K_{0.9}Na_{0.1}\left(Mg_{2.1}Fe_{2.5}Al_{0.9}\right)Al_{2.7}Ti_{0.2}Si_{5.3}O_{20}(OH)_4} +$$

$$\underset{\text{quartz}}{12.743SiO_2} + 1.087\,Ca^{2+} + 7.043\,Na^{+} +$$

$$4.052\,H^{+} \Rightarrow \underset{\text{albite}}{8.27\,Na_{0.9}Ca_{0.1}Al_{1.1}Si_{2.9}O_8} +$$

$$\underset{\text{titanite}}{0.26\,CaTiSiO_5} + 2.6\,K^{+} + 2.6\,Fe^{2+} + 2.22Mg^{2+} +$$

$$6.026\,H_2O$$

Several researchers (e.g. RUBENACH, 2005; HOLNESS, 2003; ENGVIK et al., 2008; DOLEJŠ & WAGNER, 2008) demonstrated that replacement of micas, (primarily muscovite and biotite) by albite, owing to fluid infiltration can play a significant role in alteration of crystalline rocks. The hydrothermal solution ensured Ca^{2+} transport in the alteration zone (Fig. 10, zone 1), and Ca^{2+} could be preserved as groups of small titanite crystals in the replacement albite or could be incorporated into albite. The appearance of titanite indicates that the Ti content of biotite was immobile during hydrothermal leaching. Farther away from the veins, epidotization of biotite became dominant due to the Ca^{2+}-containing fluid infiltrating the wall-rock. The continuous Ca addition in the whole altered zone is evidenced from Fig. 9, and 10. Epidotization of biotite releases K^+ and Mg^{2+} ions that were removed by the hydrothermal fluid (Fig. 9C, 10/zone 2). Significant depletion of Fe (Fig. 10, zones 1–3) indicates that during epidotization of biotite, a certain amount of iron had been removed by the fluid as Fe^{2+}. The small euhedral titanite grains that occur around and inside replacive epidote indicate that formation of epidote could not consume all of the Ca^{2+} transported by the fluid, hence Ca^{2+} was in excess during metasomatism of the wall-rock (Fig. 10).

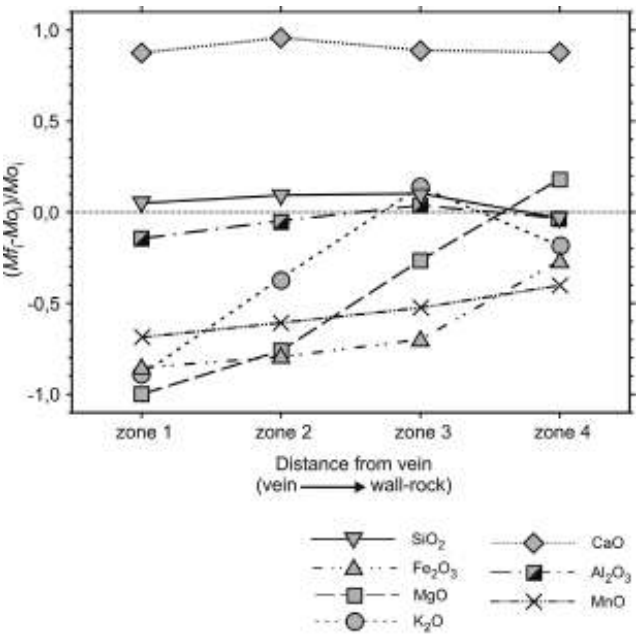

Figure 10: Diagram representing the relative mass changes of elements in order of these elements original mass as a function of distance from the propylitic veins. Dotted horizontal line at zero value indicate TiO_2 as the inert (constant mass) constituent.

In addition, titanite also contains Si, i.e. a certain amount of silica must also have been released from biotite during the alteration. Knowing the composition of all initial reactants and final products, the following reaction equation (2) can be constructed (biotite from ÁRKAI et al., 1999; epidote from FINTOR, 2005):

$$\underset{\text{biotite}}{K_{1.9}Na_{0.1}Mg_{2.1}Fe_{2.5}Al_{0.9}\left(Al_{2.7}Ti_{0.2}Si_{5.3}O_{20}\right)(OH)_4} +$$

$$3.33Ca^{2+} + 1.2524H^{+} \Rightarrow$$

$$\underset{\text{epidote}}{1.5652Ca_2\left(Al_{2.3}Fe_{0.7}\right)Si_3O_{12}OH} +$$

$$\underset{\text{titanite}}{0.2\,CaTiSiO_5} + 1.4044Fe^{2+} + 2.1\,Mg^{2+} + 1.9\,K^{+}$$

$$+0.1Na^{+} + 0.4044H_4SiO_4(aq) + 1.0348H_2O$$

Epidotization of biotite is a well-known process especially in metasomatic alterations caused by granitic and granodioritic intrusions (e.g. JACOBSEN & MCCARTHY, 1976; SINGLETON, 1979; KLEMD & BARTON, 1988; ŠARIČ, et al., 2009). From comparison of the former equation with Fig. 10 (zone 2), it is obvious that not all of the potassium had been removed from this part of the vein margin. It is likely that this deficit most probably resulted from muscovite that had not suffered epidotic or chloritic alteration and its replacement by albite became weak in the zone 2. However, sericitization became more intensive from zone 2, and a significant amount of potassium that was released during dissociation of biotite could be incorporated into sericite. Towards the unaltered wall-rock, epidotization became less effective and chloritic alteration became predominant. In a few locations of this region chlorite-pseudomorphs contain

sagenite rutile inclusions, which support the immobility of titanium in the altered rocks, but indicate that calcium and silica were insufficient to form titanite in these domains.

The Mg content in this zone (Fig. 10/zone 3) increases most obviously due to the predominance of chlorite and a lesser epidote content. The significant increase in the potassium content (Fig. 10 zone 3) can be attributed to more factors. Sericitization is the most intensive in this zone; while muscovite is almost unaltered in this part of the alteration zone, except for minor sericitic recrystallization. Although chloritization of biotite is very intensive towards the unaltered wall-rock, more and more unaltered biotite relics occur in the chloritized domains that also conserve potassium.

In zone 4, those components that display the most significant mass depletion elsewhere (Fig. 10, zones 1–3) reach their mass values characteristic of the unaltered wall-rock (Fig. 10, zone 4). Here, the major alteration mineral is sericite with a few chlorite filled cavities. The high Ca-content (Fig. 10, zone 4) of the zone is most probably due to the presence of cavity-filling epidote, which occurs very frequently in the alteration zones, and in the unaltered wall-rock.

5.2. Palaeohydrology

The euhedral albite crystals on the cavity walls, and the well-developed growth zonation of the cavity filling epidote (Fig. 4D), indicate that these minerals precipitated in an open space system. The secondary porosity was most probably caused by hydrothermal leaching of the circulating fluid, which is one of the most effective processes in the metasomatic regime (PUTNIS, 2002). Effective leaching is supported by the significant turbidity of feldspars in the altered margins, because this texture can develop by fluid infiltration (PARSONS & LEE, 2000; WALKER et al., 1995). The primary (P1, P2) and pseudosecondary (PS) fluid inclusions of cavity filling epidote, display a uniform physicochemical character, which is a dilute aqueous-electrolyte solution without any volatile components. Both the composition (0.2–1.6 mass% eq. NaCl) and the range of T_h values (200–360 °C) indicate a fluid identical to that found in the primary fluid inclusions of vein filling diopside (0.7–2.9 eq. mass % NaCl, T_h: 308–362 °C), and epidote (0.2–1.2 eq mass% NaCl, T_h: 206–359 °C), of the Ca-Al-silicate veins (FINTOR et al., 2009) that are bordered by the metasomatised zone. Based on the previous assumptions, it could be stated that an interconnected cavity system existed in the margins that was in connection with the veins. Hence the migrating fluid penetrated the cavity system resulting in epidote precipitation. Although the chemical character of the P3 assemblage (0.2–1.4 mass% eq. NaCl), indicates a similar fluid type to that found in P1 and P2, the lower T_h values (160–200 °C) indicate that trapping of this fluid type occurred later than the main phase of hydrothermal alteration. Taking into consideration that any unambiguous evidence for heterogeneous entrapment, or post-entrapment modifications of inclusions, including leakage/refilling or irreversible change of inclusion volume etc. could not be found, the wide T_h range (200–364 °C) may be explained by subsequent entrapment of primary and pseudosecondary FI in a cooling hydrothermal fluid regime. Such an important drop in temperature (~200 °C) that can be observed between P1 (T_h: 303–364 °C) and P3 (T_h: 160–200 °C) assemblages, can be imagined if the heat effect of an immediate magmatic source caused a short lived fluid flow with a very low fluid/rock ratio and the ambient rock temperature was ~180 °C.

The existence of an interconnected fluid circulation regime between the veins and the metasomatized domains indicates that the same pressure conditions (~88 MPa, FINTOR et al., 2009), which were established in the case of the Ca-Al-silicate veins, can be applied in the case of fluids migrating into the cavities. Based on this approach, the trapping temperature of fluid that entered the rock mass was in the 250–480 °C range similar to that which could have been observed in the Ca-Al-silicate veins (FINTOR et al., 2009). This is in accordance with such a kind of alteration in a hydrothermal metasomatic regime (ROBB, 2005).

Based on the observed mineral paragenesis, the estimated temperature range and the type of element mobilization, the studied alteration process belongs to the propylite metasomatic family based on the nomenclature of ZHARIKOV et al. (2007). As chemical compositions of pyrite in both the pure sulphide veins (TARNAI, 1998) and the Ca-Al-silicate veins is identical concerning the Co/Ni ratio (FINTOR et al., 2009), both vein types were formed due to post-magmatic hydrothermal processes and the studied veins represent real propylites. According to the "*T*-qualitative *pH* diagram" of metasomatic families (Fig. 11) (ZHARIKOV et al., 2007), propylite is stable around ~260–410 °C temperature and ~4.5–7 *pH* range, (grey shaded area on Fig. 11). As the dissociation of water is also temperature dependent, the neutral *pH* value becomes 5 at around 250 °C. Hence the

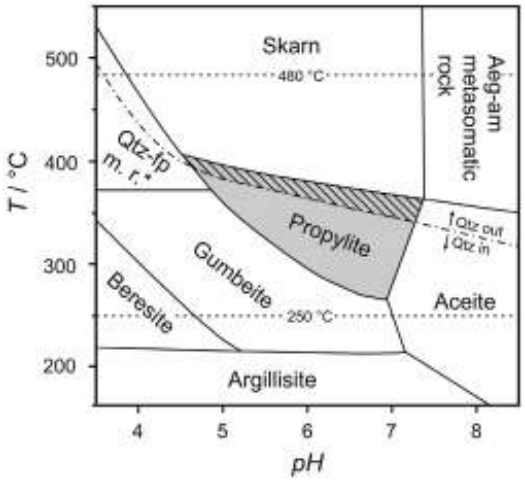

Figure 11: Diagram illustrating a fragment of the general *T*-qualitative *pH* fields of the metasomatic families (modified after ZHARIKOV et al., 2007). The dot-dash line separates acidic and neutral alkaline-alkaline families (with and without quartz). Dashed lines indicate the possible temperature range of the metasomatic alteration. The grey shaded field represents the possible metasomatic family indicated by mineral paragenesis. The hatched area indicates a metasomatic paragenesis without quartz. (Aeg-am metasomatic rock refers to aegirine-amphibolite metasomatic rock; qtz-fp m–r* refer to quartz-feldspar metasomatic rock).

observed mineral assemblage is stable at neutral-weakly alkaline conditions, which is in good agreement with observations in many other fluid-rock interaction systems where albite, epidote, and chlorite are stable (BIRD et al., 1984; GIGGENBACH, 1981; BIRD & HELGESON, 1980).

The total lack of a quartz phase in the metasomatic column indicates that the peak temperature condition of alteration was above ~340 °C, because quartz free propylite only exists at the 340–400 °C temperature range (ZHARIKOV et al., 2007) (hatched area on Fig. 11). This estimation is coherent with the fluid inclusion microthermometry data.

We can ascertain from the observed characteristics that the fluid circulated in propylitic veins (FINTOR et al., 2009), and caused significant propylitic alteration in the adjacent rocks. The composition of the metasomatic column can be summarized as *ab+ep+chl+ttn+rt+ser*. The same phases can be found inside the propylitic veins (FINTOR et al., 2009). The indications of sulphide ores in the studied well (TARNAI, 1997; 1998), and the similarities of the observed propylitic metasomatite with other fields where significant ore mineralization is associated with this type of alteration (KULIKOVA et al., 2007; TASSINARI et al., 2008; ABIA et al., 2003) indicates further investigation of the area.

6. CONCLUSIONS

1. The fluid circulated in the propylitic veins and caused metasomatism of the wall-rock with transport of considerable amount of Ca^{2+} toward the adjacent rocks. The hydrothermal leaching almost totally removed the K, Fe, Mg, and Mn basic ion content of the wall rock.
2. The characteristic mineral parageneses of individual metasomatic zones of the metasomatic column indicate that the altered wall rock is related to the propylite metasomatic family. The combined mineral assemblage of the metasomatic column is: *ab+ep+chl+ttn+rt+ser*.
3. The pervasive hydrothermal leaching in the wall-rock resulted in significant volume loss and secondary porosity in the altered domains. The fluid migration took place not only in the veins but also in the margins along them, and penetrated a great distance into the adjacent rocks along interconnected cavities.
4. The peak temperature range of the metasomatism was around 360–480 °C, and the alteration occurred as a result of a near neutral, or weakly alkaline hydrothermal solution.
5. The similarities of the studied propylitic mineral assemblages (both in the veins and in the wall-rock) with those that are characteristic in the case of many hydrothermal ore deposits, indicates further research in this topic would be useful.

ACKNOWLEDGEMENT

The authors would like to thank the Hungarian Research Fund (No. K60768) for providing financial support. The authors also would like to thank to Vesnica GARAŠIĆ, Ferenc MOLNÁR and an anonymous reviewer for their very useful and detailed reviews which contributed to the improvement of the final draft of the article. Special thanks go to Sándor Kaczur for his help during conversion of the raw element map data and to the American Journal Experts for detailed grammar checking of the manuscript.

REFERENCES

ABIA, E.H., NACHIT, H., MARIGNAC, C., IBHI, A. & SAADI, A.S. (2003): The polymetallic Au–Ag-bearing veins of Bou Madine (Jbel Ougnat,eastern Anti-Atlas, Morocco): tectonic control and evolution of a Neoproterozoic epithermal deposit.– Journal of African Earth Sciences, 36, 251–271.

ÁRKAI, P. (1985): Polymetamorphic evolution of the South-Hungarian crystalline basement, Pannonian basin: geothermometric and geobarometric data.– Acta Geologica Hungarica, 3–4/23, 165–190.

ÁRKAI, P., HORVÁTH, P. & NAGY, G. (1999): A clockwise P–T path from the Variscan basement of the Tisza Unit, Pannonian basin Hungary.– Geologica Croatica, 2/52, 109–117.

BAKKER, R.J. (2003): Package FLUIDS 1.Computer programs for analysis of fluid inclusion data and for modeling bulk fluid properties.– Chemical Geology, 194, 3–23.

BIRD, D.K., SCHIFFMAN, W., ELDERS, W.A., WILLIAMS, A.E. & MCDOWELL, D.S. (1984): Calc-Silicate Mineralization in Active Geothermal Systems.– Economic Geology, 79, 671–695.

BIRD, D.K. & HELGESON, H.C. (1980): Chemical interaction of aqueous solutions with epidote-feldspar mineral assemblages in geologic systems I. Thermodynamic analysis of phase relations in the system CaO-FeO-Fe_2O_3-Al_2O_3-SiO_2-H_2O-CO_2.– American Journal of Science, 281, 907–941.

BIRD, D.K. & HELGESON, H.C. (1981): Chemical interaction of aqueous solutions with epidote-feldspar mineral assemblages in geologic systems II. Equilibrium constraints in metamorphic/geothermal processes.– American Journal of Science, 281, 576–614.

BODNAR, R.J. (2003): Introduction to fluid inclusions.– In: SAMSON, I., ANDERSON, A. & MARSHALL, D. (eds): Fluid Inclusions: Analysis and Interpretation. Vancouver, Mineralogical Association of Canada, 1–8.

COELHO, J. (2006): GEOISO-A Windows™ program to calculate and plot mass balances and volume changes occurring in a wide variety of geologic processes.– Computers & Geosciences, 32, 1523–1528.

DE CAPITANI, C. & BROWN, T.H. (1987): The computation of chemical equilibrium in complex systems containing non-ideal solutions.– Geochimica et Cosmochimica Acta, 51, 2639–2652.

DE CAPITANI, C. (1994): Gleichgewichts-Phasendiagramme: Theorie und Software.– Beihefte zum European Journal of Mineralogy, 72. Jahrestagung der Deutschen Mineralogischen Gesellschaft, 6, 48.

DIAMOND, L.W. (2003): Systematics of H_2O inclusions.– In: IAN SAMSON, ALAN ANDERSON, & DAN MARSHALL (eds): Fluid Inclusions: Analisys and interpretation. Vancouver, Mineralogical Association of Canada, 55–77.

DOLEJŠ, D. & WAGNER, T. (2008): Thermodynamic modeling of non-ideal mineral-fluid equilibria in the system Si-Al-Fe-Mg-Ca-Na-K-H-O-Cl at elevated temperatures and pressures: Implications for hydrothermal mass transfer in granitic rocks.– Geochimica et Cosmochimica Acta, 72, 526–553.

ENGVIK, A.K., PUTNIS, A., FITZ GERALD, J.D. & AUSTRHEIM, H. (2008): Albitization of granitic rocks: The mechanism of replacement of oligoclase by albite.– The Canadian Mineralogist, 46/6, 1401–1415.

FAZEKAS, V., & VINCZE, J. (1991): Hidrotermás ércindikációk a Villány-hegység északi előtere mélyfúrásaiban [*Hydrothermal ore indications in the boreholes of the northern foreground of Villány Mountains* – In Hungarian)].– Földtani Közlöny, 91/1–4, 23–56.

FINTOR, K. (2005): Az epidotosodás vizsgálata a Baksai Komplexum képződményeiben [*Analysis of epidotization in the rock body of the Baksa Complex* – in Hungarian].– MSc thesis. Universitiy of Szeged, Szeged, 66 p.

FINTOR, K., SCHUBERT, F. & M. TÓTH, T. (2008): Hiperszalin paleofluidum áramlás nyomai a Baksai Komplexum repedésrendszerében. [*Indication of hypersaline paleofluid migration in the fracture system of the Baksa Complex* – in Hungarian].– Földtani Közlöny, 138/3, 257–278.

FINTOR, K.M. TÓTH, T. & SCHUBERT, F. (2009): A Baksai Komplexum posztmetamorf fluidum evolúciója [*Post-metamorphic fluid evolution of the Baksa Complex* – in Hungarian].– In: M. Tóth, T. (ed): Magmás és metamorf képződmények a Tiszai Egységben.– Geolitera, Szeged (in press).

GARY, M., MCAFEE, R. & WOLF, C.L. (1974): Glossary of geology. – American Geological Institute, 805 p.

GÉCZY, B. (1973): Plate tectonics and paleogeography in the East-Mediterranean Mesozoic.– Acta Geol. Hung., 27/379–389.

GIGGENBACH, W.F. (1981): Geothermal mineral equilibria.– Geochimica et Cosmochimica Acta, 45, 393–410.

GOLDSTEIN, R.H. & REYNOLDS, T.J. (1994): Systematics of fluid inclusions in diagenetic minerals, SEPM short course 31, Tulsa, Oklahoma, Society of sedimentary Geology, 199 p.

GRANT, J.A. (1986): The Isocon diagram – a simple solution to Gresen's equation for metasomatic alteration.– Economic Geology, 81/8, 1976–1982.

GRANT, J.A. (2005): Isocon analysis: A brief review of the method and applications.– Physics and Chemistry of the Earth, 30/997–1004.

GRESENS, R.L. (1967): Composition-volume relationships of metasomatism.– Chemical Geology, 2, 47–65.

GRYAZNOV, O.N. (1992): Ore-bearing metasomatic formations of folded belts. Nedra Publishing, 258 p. (In Russian).

HAAS, J. & PÉRÓ, CS. (2004): Mesozoic evolution of the Tisza Megaunit.– Int. J. Earth Sci., 93, 297–313.

HOLLAND, T.J.B. & POWELL, R. (1998): An internally consistent thermodynamic data set for phases of petrological interest.– Journal of Metamorphic Geology, 16, 309–343.

HOLNESS, M.B. (2003): Growth and albitization of K-feldspar in crystalline rocks in the shallow crust: a tracer for fluid circulation during exhumation?– Geofluids, 3/2, 89–102.

HORVÁTH, P., KOVÁCS, G. & SZAKMÁNY, GY. (2003): Eclogite and garnet amphibolite pebbles from miocene conglomerates (Pannonian basin Hungary): implications for the variscan metamorphic evolution of the Tisza Megaunit.– Geologica Carpathica, 6/54, 355–366.

JACOBSEN, J.E.B. & MCCARTHY, T.S. (1976): An unusual hydrothermal copper deposit at Messina, South Africa.– Economic Geology, 71/1, 117–130.

JAKOB, A., MAZUREK, M. & HEER, W. (2003): Solute transport in crystalline rocks at Aspo–II: Blind predictions, inverse modelling and lessons learnt from test STT1.– Journal of Contaminant Hydrology, 61, 175–190.

KASSAI, M. (1972): A Villány-Szalatnaki pleozóos mélytörés [*The Paleozoic Deep Fracture of Villány-Szalatnak* – in Hungarian].– MTA X. Oszt. Közl., 6/1, 351–354.

KIRÁLY, E. (1996): Adalékok a délkelet-dunántúli polimetamorf aljzat megismeréséhez [*New results on the research of polymetamorphic basement of South-east Transdanubia* – in Hungarian].– Földtani Közlöny, 1/126, 1–23.

KLEMD, R. (2004): Fluid Inclusions in Epidote Minerals and Fluid Development in Epidote-bearing Rocks.– Reviews in Mineralogy & Geochemistry, 56, 197–234.

KLEMD, R. & BARTON, JR.J.M. (1988): Mineralogy and Geochemistry of the Hydrothermally Altered Archean Granodioritic Rocks of the Vendersdorp Dome Western Transvaal, South Africa.– Mineralogy and Petrology, 38, 151–160.

KORZHINSKII, D.S. (1946): Metasomatic zonation near fractures and veins.– Zapiski of All-union Mineralogical Society, 75/4, 321–332, (In Russian).

KRUMGALZ, B.S., POGORELSKY, R. & PITZER, K.S. (1996): Volumetric properties of single aqueous electrolytes from zero to saturation concentration at 298.15 K Represented by Pitzer's ion-interaction equations.– Journal of Physical Chemistry Referential Data, 25, 639–663.

KULIKOVA, Z.I., SPIRIDONOV, A.M. & ZORINA, L.D. (2007): Metasomatites of the Kara gold deposit (Eastern Transbaikalia).– Russian Geology and Geophysics, 48, 901–912.

KULLERUD, K. (2000): Occurrence and origin of Cl-rich amphibole and biotite in the Earth's crust – implications for fluid composition and evolution.– In: STOBER, I. & BUCHER, K. (eds.): Hydrogeology of crystalline rocks. Dordrecht, Kluwer Academic Publishers, 205–226.

MAZUREK, M., JAKOB, A. & BOSSART, P. (2003): Solute transport in crystalline rocks at Aspo– I: Geological basis and model calibration.– Journal of Contaminant Hydrology, 61, 157–174.

MEYER, C. & HEMLEY, J., J. (1967): Wall rock alteration.– In: BARNES, H.L. (ed.): Geochemistry of hydrothermal ore depodits. Pennsylvania, University park, Holt, Reinhart and Winston, Inc., 166–235.

NADEN, J. (1996): CalcicBrine 1.5: a Microsoft Excel 5.0 add-in for calculating salinites from microthermometric data in the system NaCl-$CaCl_2$-H_2O. *PACROFI VI*, University of Wisconsin.

OMEL'YANENKO, B.J. (1978): Wall rock hydrothermal alteration. Nedra Publishing, 215 p. (In Russian).

PARSONS, I. & LEE, M.R. (2000): Alkali Feldspars as microstructural markers of fluid flow.– In: STOBER, I. & BUCHER, K. (eds.): Hydrogeology of Crystalline Rocks. Dordrecht, Kluwer Academic Publishers, 27–50.

PUTNIS, A. (2002): Mineral replacement ractions: from macroscopic observations to microscopic mechanisms.– Mineralogical Magazine, 66/5, 689–708.

RAVASZ BARANYAI, L. (1969): Eclogite from the Mecsek Mountains, Hungary.– Acta Geologica Academiae Scientiarum Hungaricae, 13, 315–322.

ROBB, J.L. (2005): Hydrothermal ore forming processes. – In: ROBB, J.L. (ed): Introduction to ore forming processes. Johannesburg, Blackwell Publishing Company, 129–214.

ROEDDER, E. (1984): Fluid Inclusions. Reviews in Mineralogy, Mineralogical Society of America, 12, 644 p.

RUBENACH, M.J. (2005): Relative timing of albitization and chlorine enrichment in biotite in proterozoic schists, snake creek anticline, Mount Isa Inlier, Northeastern Australia.– The Canadian Mineralogist, 43, 349–366.

RUSINOV, V.L. (1989): Metasomatic processes in volcanic rocks., Nauka Publishing, 214 p. (In Russian).

ŠARIČ, K., CVETKOVIČ, V., ROMER, R., L., CHRISTOFIDES, G. & KORONEOS, A. (2009): Granitoids associated with East Vardar ophiolites (Serbia, F.Y.R. of Macedonia and northern Greece): Origin, evolution and geodynamic significance inferred from major and trace element data and Sr-Nd-Pb isotopes.– Lithos, 108, 131–150.

SCHERBAN', I.P. (1975): Conditions of low temperature wall rock metasomatites formation (on example of Altai-Sayan region)., Nauka Publishing, 197 p. (In Russian).

SCHERBAN', I.P. (1996): Ore-bearing near-vein metasomatites. Lebed' Publishing, 350 p.

SIIVOLA, J. & SCHMID, R. (2007): List of Mineral Abbreviations.– In: FETTES, D. & DESMONS, J. (eds.): A classsification and glossary of terms. New York, Cambridge University Press, 93–110.

SINGLETON, D.G. (1979): Geology of the Seward Mountains, Western Palmer Land.– British Antarctic Survey Bulletin, 49, 81–89.

SZEDERKÉNYI, T. (1976): Barrow-type metamorphism int he crystalline basement of South-East Transdanubia.– Acta Geol. Ac. Sci. Hung., 20, 47–61.

SZEDERKÉNYI, T. (1979): A mecseki ópaleozos-prekambriumi alapszelvények komplex földtani feldolgozása [*Complex geological evaluation of Precambrian-Paleozoic bore-logs in the Mecsek mountain* – in Hungarian]. Manuscript., JATE, Szeged, 139 p.

SZEDERKÉNYI, T. (1983): Origin of amphibolites and metavolcanics of crystalline complexes of south transdanubia, Hungary.– Acta Geologica Hungarica, 1–2/26, 103–136.

SZEDERKÉNYI, T. (1984): Az alföld kristályos aljzata és földtani kapcsolatai [*Crystalline basement of the Great Hungarian Plain and its geological connections* – in Hungarian]. Department of Mineralogy, Geochemistry and Petrology. Szeged, University of Szeged, 184 p.

SZEDERKÉNYI, T. (1996): Metamorphic formations and their correlation in the Hungarian part of Tisia Megaunit (Tisia Composite Terrane).– Acta Mineralogica-Petrographica, Szeged, XXXVII, 143–160.

TARNAI, T. (1997): Ore minerals from the key section of the Baksa Complex (W Baranya hills, Hungary).– Acta Mineralogica-Petrographica, XXXVIII/Supplementum, 119–133.

TARNAI, T. (1998): Mineralogical-petrological study on ore vein penetrated by the key-borehole Baksa No. 2 SE Transdanubia, Hungary.– Acta Mineralogica-Petrographica, XXXIX, 21–34.

TASSINARI, G.C.C., PINZON, D.F. & VENTURA, B.J. (2008): Age and sources of gold mineralization in the Marmato mining district, NW Colombia: A Miocene-Pliocene epizonal gold deposit.– Ore Geology Reviews, 33, 505–518.

WALKER, F.D.L., LEE, M.R. & PARSONS, I. (1995): Micropores and micropermeable texture in feldspars: geological and geophysical implications.– Mineralogical Magazine, 59, 507–536.

ZHARIKOV, V.A., PERTSEV, N.N., RUSINOV, V.L., CALLEGARI, E. & FETTES, D.J. (2007): Metasomatism and metasomatic rocks. Metamorphic Rocks: A classification and glossary of terms., FETTES, D. & DESMONS, J., New York, Cambridge University Press, 58–69.

Manuscript received June 17, 2009
Revised manuscript accepted November 10, 2009
Available online February 28, 2010